Materials Research Letters

ISSN: 2166-3831 (Online) Journal homepage: www.tandfonline.com/journals/tmrl20

Magnetic order multilayering in FeRh thin films by He-Ion irradiation

S. P. Bennett , A. Herklotz, C. D. Cress, A. Ievlev, C. M. Rouleau, I. I. Mazin & V. Lauter

To cite this article: S. P. Bennett , A. Herklotz, C. D. Cress, A. Ievlev, C. M. Rouleau, I. I. Mazin & V. Lauter (2018) Magnetic order multilayering in FeRh thin films by He-Ion irradiation, Materials Research Letters, 6:1, 106-112, DOI: 10.1080/21663831.2017.1402098

To link to this article: https://doi.org/10.1080/21663831.2017.1402098

This work was authored as part of the Contributor's official duties as an Employee of the United States Government and is therefore a work of the United States Government. In accordance with 17 U.S.C. 105, no copyright protection is available for such works under U.S. Law

View supplementary material

Published online: 15 Nov 2017.

Submit your article to this journal

Article views: 2826

View related articles

View Crossmark data

Citing articles: 6 View citing articles

Full Terms & Conditions of access and use can be found at
https://www.tandfonline.com/action/journalInformation?journalCode=tmrl20

MATER. RES. LETT., 2018
VOL. 6, NO. 1, 106–112
https://doi.org/10.1080/21663831.2017.1402098

MATERIALS RESEARCH LETTERS
Taylor & Francis
Taylor & Francis Group

ORIGINAL REPORT

OPEN ACCESS
Check for updates

Magnetic order multilayering in FeRh thin films by He-Ion irradiation

S. P. Bennett [a], A. Herklotz [b], C. D. Cress [c], A. Ievlev [d], C. M. Rouleau [d], I. I. Mazin [a] and V. Lauter [e]

[a]Materials Science and Technology Division, The U.S. Naval Research Laboratory, Washington, DC, USA; [b]Materials Science and Technology Division, Oak Ridge National Laboratory, Oak Ridge, TN, USA; [c]Electronics Science and Technology Division, The U.S. Naval Research Laboratory, Washington, DC, USA; [d]Center for Nanophase Materials Science, Oak Ridge National Laboratory, Oak Ridge, TN, USA; [e]Quantum Condensed Matter Division, Neutron Sciences Directorate, Oak Ridge National Laboratory, Oak Ridge, TN, USA

ABSTRACT

The heterointerfacing of different materials with competing magnetic orders forms the basis for today's spintronic devices, however materials compatibility has remained a major limitation to the conception of new multilayered systems. Here, we uncover a multilayer of competing magnetic orders within a single layer of FeRh after low-energy He-ion irradiation: metamagnetic, ferromagnetic, and spin glass. Polarized neutron reflectometry, irradiation modeling, and density functional theory calculations reveal a direct correlation between the disorder concentration, the depth-dependent magnetic ordering, and the onset of the metamagnetic transition. Such a heterostructure opens the door to new paradigms in antiferromagnetic electronics and ultra-low-power magnetization controllability.

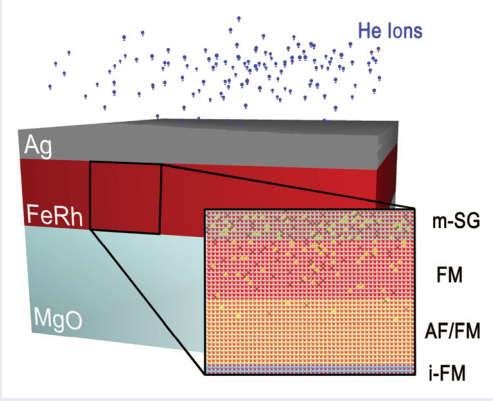

ARTICLE HISTORY
Received 31 August 2017

KEYWORDS
Metamagnetic; magnetic ordering; phase transition; antiferromagnetic; irradiation

IMPACT STATEMENT

This unlocks the possible use of intrinsic magnetism as a state-variable for logical computation via a top-down approach to the multilayering/control of magnetic order in a single metamagnetic thin film.

A route towards the active control of magnetic spin ordering at room temperature could potentially unlock a plentitude of ultra-low-power devices, ushering in the next age of high-efficiency computing. Particularly, the recently unveiled potential of antiferromagnetic (AF) electronics has spawned considerable interest in AF coupled systems for high-speed, low-power spintronics [1–3]. The metamagnetic transition from AF to ferromagnetic (FM) order in FeRh films was shown to be highly controllable by substrate strain [4–8], transition metals substitutional doping [4,5,9,10] and mesoscale patterning [11–14]. Here, we use low-energy He-ion implantation to precisely tune the metamagnetic transition temperature as a function of ion fluence (Figure 1(a)). By application of a gradient dose through the thickness, a multilayering effect in magnetic ordering is revealed with polarized neutron reflectometry (PNR). Using atomistic simulation and modeling, a direct

CONTACT S. P. Bennett steven.bennett@nrl.navy.mil Materials Science and Technology Division, The U.S. Naval Research Laboratory, Washington, DC 20375, USA

Supplemental data for this article can be accessed here. https://doi.org/10.1080/21663831.2017.1402098

This work was authored as part of the Contributor's official duties as an Employee of the United States Government and is therefore a work of the United States Government. In accordance with 17 U.S.C. 105, no copyright protection is available for such works under U.S. Law.

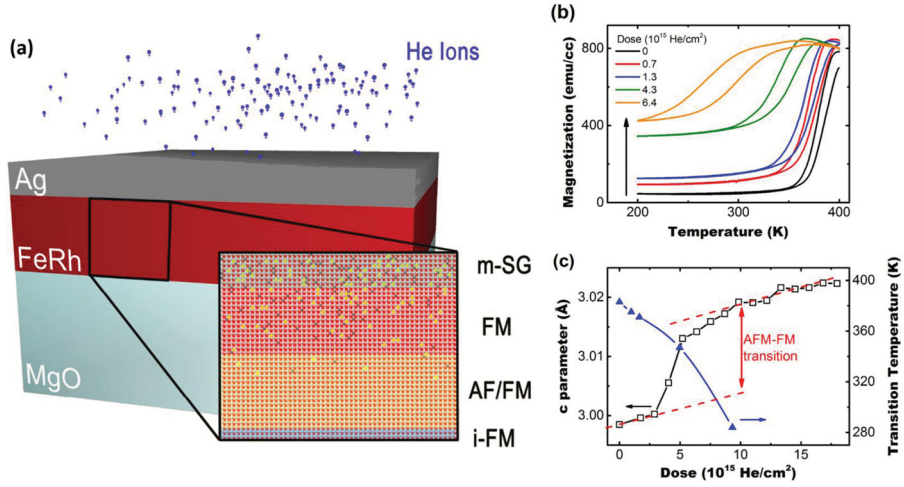

Figure 1. (a) Schematic diagram showing layered structure in gradient-dosed samples obtained from PNR measurements (m-SG = mesoscale spin glass, FM = ferromagnetic ordering, AF/FM = antiferromagnetic/ferromagnetic switchable metamagnetic ordering, i-FM = interfacial ferromagnetic ordering. (b) SQUID measurements of magnetization as a function of temperature for samples before and after He irradiation with varying doses. Arrow shows increasing background ferromagnetism with increased irradiation dose (c) (axis on the left-hand side) out-of-plane lattice constant c-parameter evolution as a function of dose measured by XRD (black squares); (axis on the right-hand side). Decreasing transition temperature with He-dose (blue triangles). Dashed lines show linear trend of c-parameter with dose in the two (AF/FM) magnetic phases.

correlation is revealed between the spin ordering and dose-induced disorder. Additionally, a thermal anneal can be used to remove implanted He atoms and repair lattice modifications from irradiation, reproducibly returning the FeRh back to a higher transition temperature state. This is in contrast to transition metal doping phase transition control methods that cannot be modified after fabrication [8,10]. On the other hand, not only the defects, but also interstitial He atoms appear to be stable in the lattice for a timespan of at least 1.5 years, despite being removable upon high-temperature annealing.

For this study, a series of epitaxial *c*-axis-oriented FeRh films ($\sim$40 nm) were grown with a Ag ($\sim$15 nm) cap as an ion stopping layer on MgO 001 crystal substrates and the films implanted ex situ with He ions, as illustrated in Figure 1(a). Recent studies using neon (20.18 u) ion implantation with an energy of 20 keV resulted in significant film damage and disorder-induced FM [15]. Here, low-energy (3.8 keV) and low-mass (4.00 u) He ions are chosen to reduce disorder and surface sputtering as well as yield a gradient vacancy profile along the film depth.

First, the influence of the He-ion irradiation on the magnetic and structural properties of the films was investigated by superconducting quantum interference device 'SQUID' magnetometry and X-ray diffraction (XRD), respectively. Magnetization measurements in Figure 1(b) show a highly tunable transition temperature as a function of dose. Displayed in Figure 1(c) is the result of room temperature XRD on the FeRh's 001 peak position as a function of implantation dose. The data clearly reveal the FeRh unit cell expansion upon He implantation due to the onset of the FM phase as the AF/FM transition temperature is shifted below room temperature (Figure 1(c)). However, while we do see a highly controllable decrease in the metamagnetic transition temperature, the magnitude of the transition is decreased and its width is increased. More importantly, along with this tunable phase transition there persists an anomalous FM background that increases in magnitude as the dose is increased. From thermomagnetic M vs. T measurements this is evident as an increase in the magnitude of the magnetization below the transition temperature and nominally in the AF phase (see black arrow in Figure 1(b)). Previous measurements of irradiated FeRh films with traditional magnetometer techniques have witnessed a similar FM background ordering [15–18].

From previous experiments and the SQUID measurements shown here, one can infer that both magnetic phases (FM and metamagnetic) of FeRh are present in ion-irradiated films. However, the origin of the FM is still largely unexplored. A similar persistence of FM below the transition temperature for undosed films has been recently interpreted as interfacial magnetization at the bottom and top of the film, attributed to epitaxial and surface strain [7,8,19]. However, in He-implanted samples, the apparent controllability of this FM ordering lends to question the nature of this phenomenon in irradiated samples [15,16,20]. Traditional magnetometry can only measure the total magnetization of the specimen, providing no insight into the spatial, interfacial, or strain-driven origins of these thermomagnetic effects. PNR allows the determination of magnetization profiles and is thus an

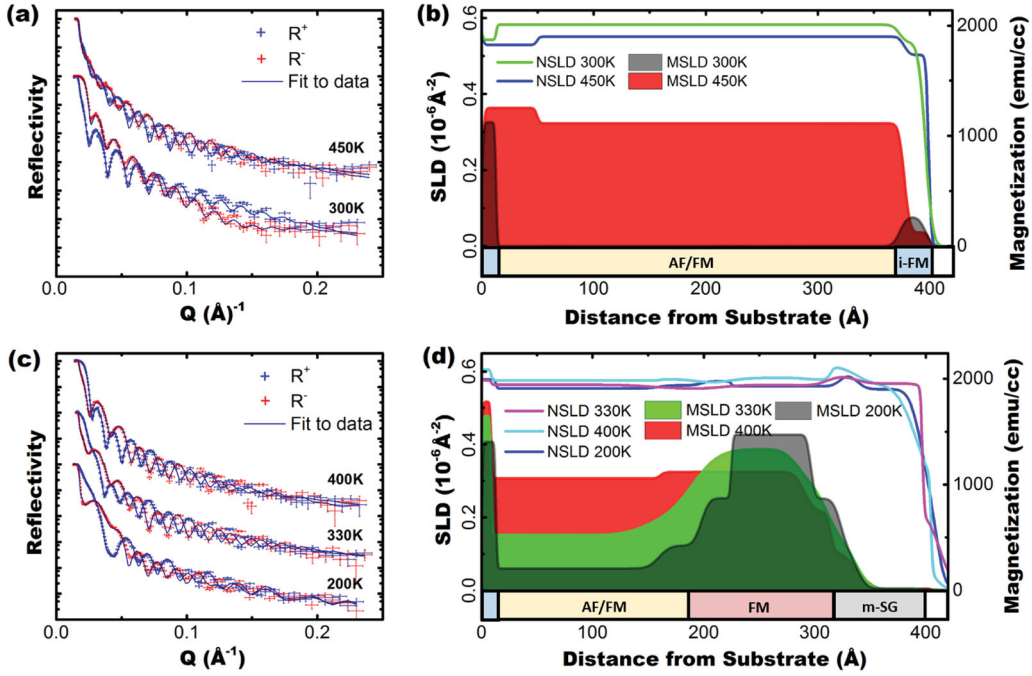

Figure 2. (a) PNR reflectivities of virgin (undosed) samples of FeRh grown on MgO 300 K (below metamagnetic transition) and 450 K (above metamagnetic transition). Blue lines show fit through the data. Overlaid red and blue error bars show data points for positive and negative neutron polarizations, respectively. (b) MSLD and NSLD depth profiles of a virgin FeRh film extracted from fits to data in Figure 2(a). (c) PNR reflectivity of FeRh sample after He-ion irradiation at 400 K (above transition), 330 K (within the transition region), and 200 K (below the transition). (d) MSLD and SLD depth profiles of irradiated FeRh film taken from fits in Figure 2(c).

ideal tool to study depth-sensitive magnetic order in epitaxial thin films. Here, we have used PNR at temperatures above, below, and in the middle of the phase transition in order to explore the effects of He-ion irradiation on FeRh films.

Experimental data using the PNR technique on both virgin and implanted FeRh films are shown in Figure 2(a,d). Strikingly, for the dosed film these measurements show a clear coexistence of both a stabilized FM layer at some depth below the surface, and a metamagnetic (AF/FM) transitional region just below that (Figure 2(d)). The stabilized FM ordering layer persists at all temperatures measured (similar to the interfacial FM layers previously described), while the layer directly below has a decreased metamagnetic transition temperature ($T_{\mathrm{AF-FM}}$). Additionally, there is a surface layer whose magnetic ordering has been lost completely at all temperatures. Shown in Figure 4 are helium ion range and Fe/Rh displacement depth profiles obtained from TRIM/SRIM (transport/stopping and range of ions in matter) simulations. This, along with corroborated evidence from SIMS (secondary ion mass spectroscopy) analysis in supplemental Figure S1, confirms the existence of a gradient in He concentration as a function of depth, with the largest concentration at the surface of the sample. However, the concentration of Fe displacements (d_{Fe}) and Rh displacements (d_{Rh}) is 10–50 times larger than that of implanted He ions, making it likely that the observed modifications of physical properties are overwhelmingly due to the metal vacancies and interstitial ions. Regardless of the origin, the three distinct layers of magnetic ordering are correlated with both the He concentration and displacement density within the FeRh layer. Above 2×10^3 vacancies/cm^3 no magnetic ordering is detected, from $\sim 1 \times 10^3$ to $\sim 2 \times 10^3$ there exists a persistent FM ordering, and below $\sim 1 \times 10^3$ we observe the metamagnetic AF/FM transitional region (whose transition temperature has been reduced, on average, to ~ 330 K).

Unlike substitutional doping to control FeRh's transition temperature [8,10], modifications to the lattice due to He irradiation can be reversed by high-temperature annealing, which heals the defects created by irradiation. To explore this further, we have annealed the irradiated film at the highest temperature available in the neutron beamline cryostat in high vacuum (450°C) for 3 h and performed PNR (Figure 3(a)). As expected, the magnetic profile in the annealed film has moved towards the surface, reflecting gradual healing. The transition temperature in the metamagnetic region has increased (Figure 3(c)), and the FM background was suppressed, as witnessed by the residual magnetic moment below the transition temperature. PNR measurements were also taken above (400 K), below (200 K), and in the middle

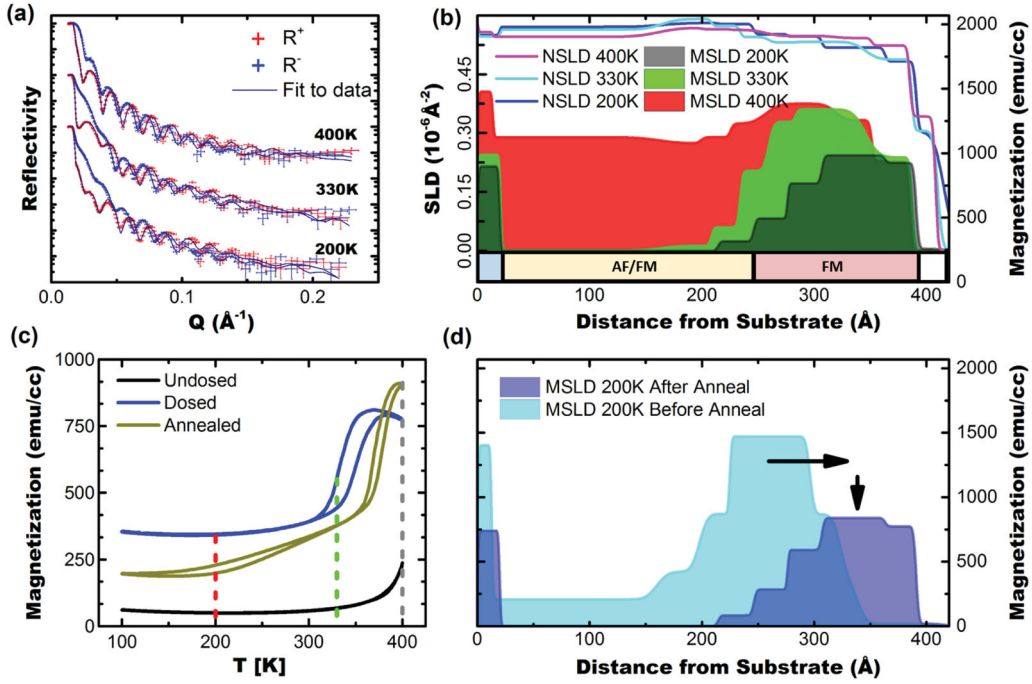

Figure 3. (a) PNR reflectivities of a gradient-dosed FeRh sample (same as from Figure 2(b,c)) after a 3 h 400 K anneal taken at the same temperatures. Blue lines show fits to the data. Overlaid red and blue error bars show positive and negative neutron polarizations, respectively. (b) MSLD and NSLD depth profiles extracted from fits to data shown in (a). (c) SQUID data showing comparison of irradiated FeRh film before and after annealing. Dashed lines indicate temperatures at which PNR in Figure 3(b) were performed (d) 200 K comparison of SLD and MSLD depth profiles before and after anneal. Arrows show migration of an FM region to the surface of the sample and decrease in magnetization magnitude, as the irradiation-induced defects are being annealed.

(330 K) of the AF/FM transition in the annealed samples (Figure 3(a,b)). Consistent with the above reasoning, the FM region was shifted towards the surface of the film, starting directly at the surface interface, supplanting the highly disordered spin-glass region.

Results and discussion

Our XRD data in Figure 1(c) illustrate the irradiation-induced switching of the magnetic order and the volume effect of the metamagnetic transition. When the He-ion fluence reaches a critical value, the magnetic order changes from AF to FM by a first-order transition, with a 1% expansion in volume. To estimate the irradiation-induced damage in the system, we have run SRIM simulations (Figure 4). According to the relative concentration profile of He atoms to vacancies in Figure 4, an interstitial He-induced quasi-uniaxial strain forcing the 1% larger volume FM state due to implanted He atoms would make a rather small effect. Rather, the temperature behavior of the persistently FM layer must be related to the disorder, namely to Frenkel pairs (i.e. a vacancy and its interstitial atom) in the Fe and Rh sublattices. As a result of gradient vacancy profile, the bottom portion of the film was subjected to the lowest dose, and it exhibits FeRh's typical metamagnetic behavior. This region has

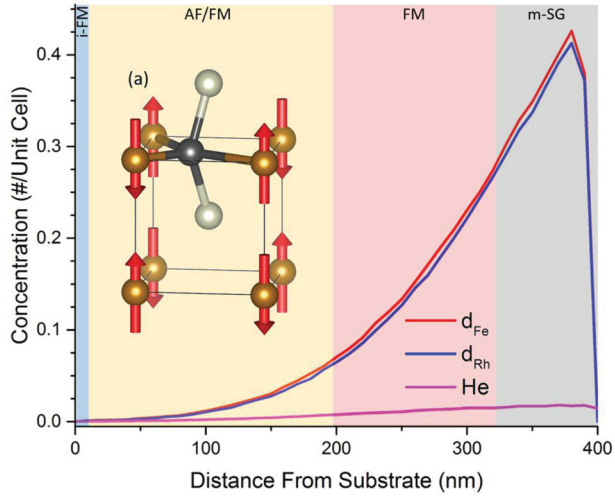

Figure 4. Concentration of Fe and Rh atoms displaced into interstitial positions and of He ions stopped in the bulk, as a function of distance from the substrate (0 Å is the interface with the MgO substrate and at 390 Å is the interface with the capping Ag layer), as simulated by TRIM/SRIM modeling. (a) Sketch shows an example of magnetic disorder introduced by a displaced Fe atom (black ball). The brown balls indicate surrounding Fe atoms which assume the overall antiferromagnetic order, and the silver ones are Rh (sketch assumes zero lattice relaxation).

a lower temperature AF/FM transition, which is tunable in this small dose regime as shown in Figure 1(b,c) by magnetometry measurements. The middle portion

experienced a moderately higher dose and developed a persistent FM state. The topmost portion that received the highest dose and developed the largest amount of disorder has lost its magnetic ordering entirely; as will be discussed below, we believe it to be in a spin glass state, or 'mesoscopic spin glass' (m-SG).

Let us now discuss the ordered layers in more detail. As one progresses from the substrate towards the top of the film, the first several atomic layers exhibit robust ferromagnetism. Additionally, PNR measurements conducted on a film grown with metallic buffer layers and a high degree of lattice match also show such an interfacial FM (i-FM) [8]. This i-FM effect is present before and after irradiation, so it is clearly triggered by interaction with substrate and has been documented in previous reports [7,8,19]. This effect is far from trivial. Both from the Clapeyron–Clausius equation, and from results of pressure experiments [21], the compressive strain exhorted by the MgO substrate should stabilize the AF state rather than the FM. Thus, the effect of the interface goes far beyond simple strain. There are extensive debates in the literature [7–9,19,22], and the issue has not been settled with certainty; for the purpose of this paper, however, we shall concentrate on the effects of irradiation-induced disorder away from the interface with the substrate.

The disordered middle region of the film exhibits an FM state that is stable in the entire temperature range investigated. The exact origin of this FM state cannot be uncovered without detailed theoretical modeling. We can, however, point out a very general reason for moderate disorder to favor FM ordering. As observed before [23–26], direct Fe–Fe interaction is AF, however, in the AF structure Rh remains, by symmetry, nonmagnetic. Furthermore, in the FM state, Fe induces a net polarization on the Rh atoms of the order of 1 μ_B. This gives an additional energy gain, commonly referred to as the Hund's rule coupling (atomic physics), or the Stoner energy (density functional theory [DFT]). The latter can be estimated [27] as $IM^2/4$, where I is the so-called Stoner parameter of the exchange-correlation strength, which for the 4d metals is $\sim$0.4 eV. Thus, the Stoner energy is $\sim$100 meV per unit cell for Rh in FeRh. This is at least twice as large as the calculated energy difference between the AF and FM ground states of FeRh at zero temperature (see Figure S2). As a result, the two types of Fe–Fe interactions (direct AF, and FM mediated by Rh) are of the same order and in close competition making them prone to transition between either state by disorder.

Importantly, even though both ground states are at similar energies, they respond differently to the disorder. Indeed, the AF structure on the simple cubic lattice is not frustrated: all nearest neighbor bonds are AF and provide equal contribution to the AF energy gain (which is $3J_{\mathrm{Fe-Fe}}$ per unit cell). Removing one Fe atom leaves behind a vacancy, thus removing four AF bonds and increasing the energy by $6J_{\mathrm{Fe-Fe}}$. It further creates an interstitial Fe atom with a tetrahedral symmetry (see Figure 4), which disrupts the magnetic interactions of three neighboring Fe. Thus, the impact of disorder on the AF structure is strong. On the other hand, disorder has little effect on the FM coupling mediated by Rh; even in the neighborhood of an Fe vacancy or an interstitial Fe, as long as all Fe spins are parallel, Rh acquires about the same magnetic moment without any loss of the Stoner energy. The same is true for a displaced Rh. Therefore, disorder is injurious for the AF order, while the FM order is indifferent to moderate disorder. Therefore, the energy balance for moderate irradiation doses shifts towards the FM ordering and, as observed in our experiment, the higher irradiation dose results in a higher rate of displaced Fe atoms that favors a shift of AF $\rightarrow$ FM transition to lower in temperature. When more than 5% of all atoms (half of which are Fe) are displaced, the transition is suppressed in the entire temperature range accessed in our experiment, rendering the sample effectively FM.

The surface of the film, which was exposed to the largest irradiation dose, displacing more than 10% of Fe/Rh metal ions and leaving behind vacancies, appears entirely nonmagnetic to PNR. A similar behavior has been witnessed in the past in bulk samples of FeRh by introduction of lattice defects by high-energy ball milling [28,29]. While Rh moments are fragile, Fe magnetism is very strong locally. Computational tests using the standard Vienna Ab initio Simulation Package (VASP) code [30] to displace one Fe to a far removed interstitial location, verifies that it remains magnetic with a moment in excess of 2 Bohr magnetons. Complete absence of the net magnetization signifies that Fe moments are completely disordered, which may occur either in paramagnetic or in a spin-glass state. Since the material experiences a sharp transition into a FM state with $\sim$10% of vacancies isothermally (XRD from Figure 1(c) and SRIM from Figure 4) [15,16], a paramagnetic ordering is less probable, and a freezing of Fe spins with zero net magnetization is more likely. Ostensibly, this contradicts the previous argument that disorder favors FM. Important to note however that, when the concentration of Rh vacancies is large enough, extended Rh-depleted regions are created where AF coupling dominates. Here, the system freezes into a collection of FM clusters, whose orientation varies, but is fixed with respect to each other by inter-cluster regions where the AF coupling dominates (Figure S2). These evidences conclude that the top 100–150 Å of our irradiated film are converted into a so-called mesoscopic spin glass, to distinguish it from typical spin glasses

formed by magnetic ions with completely random orientations [31,32].

Conclusions

Using polarized neutrons, SRIM modeling, and DFT analysis, we have uncovered the depth-dependent nature of magnetization modifications in He-ion-irradiated FeRh thin films, revealing an irradiation gradient-induced multilayer of magnetic spin orderings. Fitting a model to polarized neutron reflectivity profiles at temperatures above, below and in the middle of the metamagnetic transition has uncovered the existence of a persistently FM layer, previously only evident in the high magnetization background of thermomagnetic measurements. We have also demonstrated how the high-temperature metamagnetic transition can be restored using high-temperature thermal annealing, and used PNR to show how this causes stabilization of an FM region closer to the surface interface, and a disorder-induced mesoscopic spin glass immediately below the surface, in the most highly irradiated layer. These discoveries can be used to form a multilayer of AF, FM, spin glass, or metamagnetic layers, opening new paradigms in vertically patterned AF spintronics. Additionally, these layers will exhibit different resistivities [3], and strain sensitivity [4,7] leading towards ultra-low-power tunable AF electronics [4,33].

Experimental

Sample growth: FeRh samples $\sim$ 40 nm thick were grown using magnetron sputtering from a stoichiometric FeRh target at 630°C in a 1.5-mTorr Ar atmosphere. They were then annealed *in situ* for 1 h at 730°C before being cooled to 240°C and depositing a $\sim$30-nm Ag capping/stopping layer to prevent oxidation during transport, surface damage from irradiation and promote good uniform He-dosing to the buried FeRh layer. The samples were then irradiated at 3.8 keV with He^+ ions. Irradiation sputtering of the Ag protection layer left behind some residual Ag, which was removed before PNR measurement.

PNR experiments: PNR [34,35] experiment was performed on the Magnetism Reflectometer [34] at the Spallation Neutron Source at Oak Ridge National Laboratory [35]. It is a time-of-flight instrument with a wavelength band of $\lambda \sim 2.6$–8.6 Å of highly polarized neutrons (98.5%). During the experiment an external magnetic field of 0.5 T is applied in-plane, saturating the sample parallel to the neutron polarization.

The experiential data are used to extract the depth profile of the neutron scattering length density (NSLD). The depth dependence of the SLD profile is obtained by fitting the reflectivity data. From the fit to the two reflectivity curves (R^+ and R^-), the depth-dependent nuclear (Nb_n) and magnetic (Nb_m) scattering length density profiles (NSLD and MSLD), respectively, are determined. In particular, when measuring at magnetically saturated state, the MSLD (Nb_m) obtained is linked to M_s [36] and allows its direct evaluation. The magnetic scattering length density MSLD (or Nb_m in Equation (1)) can be converted to the physical magnetization (M) in the cgs units, M (emu/cm^3) $= 3.5 \times 10^8\, Nb_m$ (Å^{-2}).

The reflectivity data were fit with Python-based software GenX [37]. Fitting of the reflectivity data is performed first with the minimum number of parameters (substrate, film, and surface layer). Each layer is described with three parameters (NSLD, MSLD, and thickness). The model is then refined by successively adding sublayers to fit the details of the magnetic and nuclear structure until a good statistical fit to the data is achieved (10 layers total). The fit of R^+ and R^- was performed simultaneously for each temperature dataset (shown in Figure 2(a,b) and Figure 3(a)). The estimated error is not exceeding 5% of the obtained parameter values.

Computational

The DFT calculations reported in this paper were performed using the projector augmented wave method [38] as implemented in the VASP [24], using pseudopotentials with the p-states in the valence window. Results for the single-cell were verified by all-electron linearized augmented plane wave (LAPW) calculations (as implemented in the WIEN2K package [39]). In all cases, the Perdew–Burke–Ernzerhof exchange-correlation potential was employed [40].

Disclosure statement

No potential conflict of interest was reported by the authors.

Funding

This work was supported by the Scientific User Facilities Division, the Office of Basic Energy Sciences (BES), US Department of Energy (DOE), (S.P.B., V.L., C.R.), and by Office of Naval Research through the NRL basic research program (S.P.B., C.C., and I.I.M.). This effort was also supported in part by the US Department of Energy (DOE), Office of Basic Energy Sciences (BES), Materials Sciences and Engineering Division, (A.H.).

ORCID

S. P. Bennett http://orcid.org/0000-0003-2615-6321

References

[1] Wadley P, Howells B, Železný J, et al. Electrical switching of an antiferromagnet. Science. 2016;351:587–590.

[2] Marti X, Fina I, Frontera C, et al. Room-temperature antiferromagnetic memory resistor. Nat Mater. 2014;13:367–374.
[3] Lee Y, Liu ZQ, Heron JT, et al. Large resistivity modulation in mixed-phase metallic systems. Nat Commun. 2015;6:5959.
[4] Cherifi RO, Ivanovskaya V, Phillips LC, et al. Electric-field control of magnetic order above room temperature. Nat Mater. 2014;13:345–351.
[5] Le Graët C, Charlton TR, McLaren M, et al. Temperature controlled motion of an antiferromagnet- ferromagnet interface within a dopant-graded FeRh epilayer. APL Mater. 2015;3:1–8.
[6] Barua R, Jimenez-Villacorta F, Shield JE, et al. Nanophase stability in a granular FeRh-Cu system. J Appl Phys. 2013;113:1–3.
[7] Bennett SP, Wong AT, Glavic A, et al. Giant controllable magnetization changes induced by structural phase transitions in a metamagnetic artificial multiferroic. Sci Rep. 2016;6:K79.
[8] Bennett SP, Ambaye H, Lee H, et al. Direct evidence of anomalous interfacial magnetization in metamagnetic Pd doped FeRh thin films. Sci Rep. 2015;5:9142.
[9] Kinane CJ, Loving M, De Vries MA, et al. Observation of a temperature dependent asymmetry in the domain structure of a Pd-doped FeRh epilayer. New J Phys. 2014;113:1–6.
[10] Barua R, Jiang X, Jimenez-Villacorta F, et al. Tuning the magnetostructural phase transition in FeRh nanocomposites. J Appl Phys. 2013;113:23910.
[11] Aschauer U, Braddell R, Brechbühl SA, et al. Strain-induced structural instability in FeRh. Phys Rev B. 2016;94:1–10.
[12] Xie Y, Zhan Q, Shang T, et al. Effect of epitaxial strain and lattice mismatch on magnetic and transport behaviors in metamagnetic FeRh thin films. AIP Adv. 2017;7:56314.
[13] Taniyama T. Electric-field control of magnetism via strain transfer across ferromagnetic/ferroelectric interfaces. J Phys Condens Matter. 2015;27:504001.
[14] Uhlíř V, Arregi JA, Fullerton EE. Colossal magnetic phase transition asymmetry in mesoscale FeRh stripes. Nat Commun. 2016;7:13113.
[15] Heidarian A, Bali R, Grenzer J, et al. Tuning the antiferromagnetic to ferromagnetic phase transition in FeRh thin films by means of low-energy/low fluence ion irradiation. Nucl Instrum Methods Phys Res Sect B Beam Interact. Mater. Atoms. 2015;358:251–254.
[16] Koide T, Satoh T, Kohka M, et al. Magnetic patterning of FeRh thin films by energetic light ion microbeam irradiation. Jpn J Appl Phys. 2014;53:05FC06.
[17] Menéndez E, Liedke MO, Fassbender J, et al. Direct magnetic patterning due to the generation of ferromagnetism by selective ion irradiation of paramagnetic FeAl alloys. Small. 2008;5:229–234.
[18] Ohtani Y, Hatakeyama I. Antiferro-ferromagnetic transition and microstructural properties in a sputter deposited FeRh thin film system. J Appl Phys. 1993;74:3328–3332.
[19] Fan R, Kinane CJ, Charlton TR, et al. Ferromagnetism at the interfaces of antiferromagnetic FeRh epilayers. Phys Rev B – Condens Matter Mater Phys. 2010;82:1–6.
[20] Bali R, Wintz S, Meutzner F, et al. Printing nearly-discrete magnetic patterns using chemical disorder induced ferromagnetism. Nano Lett. 2014;14:435–441.
[21] Vinokurova LI, Vlasov AV, Pardavi-Horváth M. Pressure effects on magnetic phase transitions in FeRh and FeRhIr alloys. Physica Status Solidi (b). 1976;78:1–9.
[22] Baldasseroni C, Pálsson GK, Bordel C, et al. Effect of capping material on interfacial ferromagnetism in FeRh thin films. J Appl Phys. 2014;115:43919.
[23] Gruner ME, Hoffmann E, Entel P. Instability of the rhodium magnetic moment as the origin of the metamagnetic phase transition in $\alpha-$FeRh. Phys Rev B. 2003;67:64415.
[24] Witte R, Kruk R, Gruner ME, et al. Tailoring magnetic frustration in strained epitaxial FeRh films. Phys Rev B – Condens Matter Mater Phys. 2016;93:1–9.
[25] Sandratskii LM, Mavropoulos P. Magnetic excitations and femtomagnetism of FeRh: A first-principles study. Phys Rev B. 2011;83:174408.
[26] Gu RY, Antropov VP. Dominance of the spin-wave contribution to the magnetic phase transition in FeRh. Phys Rev B – Condens Matter Mater Phys. 2005;72:1–4.
[27] Andersen OK, Madsen J, Poulsen UK, et al. Magnetic ground state properties of transition metals. Phys B+C. 1977;86–88:249.
[28] Hernando A, Navarro E, Multigner M, et al. Boundary spin disorder in nanocrystalline FeRh alloys. Phys Rev B. 1998;58:5181–5184.
[29] Navarro E, Multigner M, Yavari AR, et al. The spin glass state of metastable fcc FeRh. Europhys Lett. 1996;35:307–312.
[30] Kresse G, Furthmüller J. Efficient iterative schemes for ab initio total-energy calculations using a plane-wave basis set. Phys Rev B. 1996;54:11169–11186.
[31] Mydosh JA. Spin glasses: an experimental introduction. Chicago: Taylor & Francis. 1993; 256 p.
[32] Motohashi T, Caignaert V, Pralong V, et al. Competition between ferromagnetism and spin glass: the key for large magnetoresistance in oxygen-deficient perovskites SrCo1-xMxO3-δ (M = Nb,Ru). Phys Rev B – Condens Matter Mater Phys. 2005;71:1–8.
[33] Fina I, Quintana A, Padilla-Pantoja J, et al. Electric-Field-Adjustable time-dependent magnetoelectric response in martensitic FeRh alloy. ACS Appl Mater Interfaces. 2017;9:15577–15582.
[34] Lauter V, Ambaye H, Goyette R, et al. Highlights from the magnetism reflectometer at the SNS. Phys B Condens Matter. 2009;404:2543–2546.
[35] Felcher GP, Hilleke RO, Crawford RK, et al. Polarized neutron reflectometer: a new instrument to measure magnetic depth profiles. Rev Sci Instrum. 1987;58:609–619.
[36] Felcher GP. Polarized neutron reflectometry – a historical perspective. Physica B 1999;268:154–161.
[37] Björck M, Andersson G. Genx: An extensible X-ray reflectivity refinement program utilizing differential evolution. J Appl Crystallogr. 2007;40:1174–1178.
[38] Blöchl PE. Projector augmented-wave method. Phys Rev B. 1994;50:17953–17979.
[39] Blaha P, Schwarz K, Madsen GKH. WIEN2K, an augmented plane wave+ local orbitals program for calculating crystal properties. Vienna: TU Wien; 2001. ISBN 3-9501031-1-2. 2001;2:254.
[40] Perdew JP, Burke K, Ernzerhof M. Generalized gradient approximation made simple. Phys Rev Lett. 1996;77:3865–3868.